Mean temperature scalings in compressible wall turbulence

Cheng Cheng [1,2] and Lin Fu [1,3,4,5,*]

^{1}*Department of Mechanical and Aerospace Engineering,*
The Hong Kong University of Science and Technology, Clear Water Bay, Kowloon, Hong Kong
^{2}*Institute for Advanced Study, The Hong Kong University of Science and Technology,*
Clear Water Bay, Kowloon, Hong Kong
^{3}*Department of Mathematics, The Hong Kong University of Science and Technology,*
Clear Water Bay, Kowloon, Hong Kong
^{4}*HKUST Shenzhen-Hong Kong Collaborative Innovation Research Institute, Futian, Shenzhen 518045, China*
^{5}*Center for Ocean Research in Hong Kong and Macau (CORE),*
The Hong Kong University of Science and Technology, Clear Water Bay, Kowloon, Hong Kong

In the present study, we report a Mach number invariant function (ϕ_S) for the mean temperature field in compressible wall turbulence. We demonstrate its validation by comparing it with the invariant functions derived in the previous studies—the semilocal-type (ϕ_{SL}) and van Driest-type (ϕ_{VD}) scalings—case by case. To be specific, ϕ_{SL} works well in the inner layer of compressible channel flows with isothermal walls; ϕ_S works well in the inner layer of compressible channel flows with adiabatic walls, and supersonic/hypersonic turbulent boundary layers with cold walls; and ϕ_{VD} does not work the best among all three functions in the flows under consideration. The proposed temperature transformations based on ϕ_S show an improvement in channel flows over adiabatic walls and supersonic/hypersonic turbulent boundary layers with cold walls. The effects of the generated high-order terms during derivation are also clarified. These findings may be revealing for the development of the near-wall model in high-speed aerodynamics.

I. INTRODUCTION

It is well known that one of the most important properties of incompressible wall turbulence is the law of the wall. The distributions of the mean streamwise velocities of high-Reynolds-number wall-bounded turbulent flows versus the wall-normal coordinate (*y*) exhibit nearly universal wall-normal profiles when they are scaled with the wall quantities (denoted by a superscript plus sign, and the variables scaled by the semilocal scales are denoted by a superscript asterisk) and form the so-called log region. Inspired by the Reynolds analogy, the mean temperature profiles in low-speed turbulent boundary layers are also discovered to exhibit the logarithmic scaling [1], which takes the form

$$\frac{\bar{\theta}}{\theta_\tau} = \frac{1}{\kappa_t} \ln(y^+) + B, \tag{1}$$

where $\theta = T - \overline{T}_w$, i.e., the difference between the temperature at a given wall-normal position and the mean wall temperature, κ_t is a constant and roughly equivalent to 0.459 [2], *B* is another constant determined by the Prandtl number Pr, and $\theta_\tau = \bar{q}_w/(\bar{\rho}_w c_p u_\tau)$ with q_w, ρ_w, u_τ, and c_p being the

---

*Corresponding author: linfu@ust.hk

heat flux on the wall ($\lambda \frac{d\bar{\theta}}{dy}|_w$, λ is the molecular conductivity), the fluid density on the wall, the wall friction velocity, and the specific heat at constant pressure, respectively. However, when high-speed flows are taken into account, the situation is more complicated [3–5]. First, the compressibility leads to the remarkable viscous heating in the boundary layer, which results in the modification of the Reynolds analogy. As a result, the scaling (1) is not valid. Second, for compressible flows over adiabatic walls, θ_τ cannot be mathematically defined, and thus Eq. (1) also faces a challenge.

Inspired by the Morkovin's hypothesis [6], numerous studies have been dedicated to developing a transformation to map the compressible mean streamwise velocity profiles to their incompressible counterparts and recovering the law of the wall, and thus continued progress has been made in return [7–14]. As for the temperature scaling, however, far less attention has been paid. Patel *et al.* [15] proposed a flow-property independent function for the mean scalar field in variable property turbulent channel flows at low Mach numbers, which can be employed to construct a transformation scheme. However, the non-negligible viscous heating in high-speed flows results in the invalidation of such a scheme [16]. Very recently, Chen *et al.* [17] derived two kinds of mean temperature transformations for high-speed flows over the isothermal and adiabatic walls with monotonic temperature distributions, by following the logic of the established velocity transformations deduced by van Driest [7] and Trettel and Larsson [9], respectively (for details refer to Sec. II). These two schemes are validated by their self-built database of the Couette flows and named the van Driest-type and semilocal-type transformations, respectively. However, the accuracies of these schemes in different zones of boundary layers with distinct wall thermal boundary conditions have not been scrutinized. This is one of the objectives of the present work.

On the other hand, it is documented that both of these two types of velocity transformations do not work well in some cases. To be specific, in diabatic boundary layers and channel flows, the van Driest-type scaling cannot recover the incompressible law of the wall [9,12]. Similarly, the semilocal-type scaling fails in the log region of the boundary layers with heat transfer [12,18,19]. Would the corresponding transformations for mean temperature field fail under some circumstances? It motivates us to take a new look at the transformations related to the temperature field. Intrinsically, developing such transformations for both mean velocity and temperature fields is equivalent to uncovering the Mach number invariant functions in different regions of the turbulent boundary layers [10,12]. Hence, in the present study, we will evaluate the corresponding Mach invariant functions (semilocal type and van Driest type) for the temperature field by resorting to the open-source data from direct numerical simulations (DNS) with various Mach numbers and wall thermal boundary conditions extensively. We will also propose a Mach number invariant function for the log region of the flows and construct temperature transformations based on it. The current study not only can deepen our understanding of the basic characteristics of compressible wall turbulence, but also is of unique significance for near-wall modeling. Though simple algebraic relations connecting the mean velocity and temperature in compressible flow have been developed, such as the Crocco-Busemann formula and its modified versions [20–24], their employment for modeling purposes is impeded by one factor, namely, it requires as input the velocity and temperature at the boundary-layer edge due to its requirement of recovery temperature and edge velocity. For the complex flows, it is rather difficult to determine the boundary edge, and extra approaches have to be developed to estimate the values at the boundary-layer edge [25,26]. There is no doubt that it enhances the complexity of the model. Additionally, in a standard wall-modeled large-eddy simulation, the velocity and temperature in the log region are often treated as the inputs for a near-wall model [3,4,27]. Thus, uncovering the scaling of the mean temperature in the inner layer of compressible wall turbulence is beneficial for developing such a near-wall model for the temperature field, which is independent of the values of the velocity and temperature at the boundary-layer edge.

II. MACH NUMBER INVARIANT FUNCTIONS

Before exhibiting the results of the present study, it is of significance to state our perspective on turbulence modeling. That is, it is necessary to maintain the conciseness of the scalings. In light of this, we try to avoid the involvement of the high-order terms in deducing the mean temperature scalings. On the one hand, some existing open-source data do not contain these statistics, thus providing difficulties for in-depth investigation of their relationship with the mean temperature. On the other hand, more importantly, reserving these high-order terms impairs the conciseness of the scalings and is not beneficial for turbulence modeling. However, as we show below, for several cases, the abandonment of some high-order correlations would have non-negligible effects on the accuracy of the deduced scalings. We will clarify them as much as possible.

Let us start with the total energy equation. Both the Reynolds (denoted as $\bar{\phi}$) and the Favre averaged (denoted as $\widetilde{\phi} = \overline{\rho\phi}/\overline{\rho}$) statistics are used in the present study. The corresponding fluctuating components are represented as ϕ' and ϕ'', respectively. Assuming that the flow is statistically steady, the two-dimensional energy equation can be cast as [28,29]

$$\frac{\partial(\bar{\rho}\tilde{H}\tilde{u})}{\partial x} + \frac{\partial(\bar{\rho}\tilde{H}\tilde{v})}{\partial y} = \frac{\partial}{\partial x}(\bar{q}_x - \overline{\rho H''u''} + \overline{u\tau_{xx}} + \overline{v\tau_{yx}}) + \frac{\partial}{\partial y}(\bar{q}_y - \overline{\rho H''v''} + \overline{u\tau_{xy}} + \overline{v\tau_{yy}}), \quad (2)$$

where u, v, and H represent the instantaneous streamwise velocity, the wall-normal velocity, and the total enthalpy ($H = c_p T + \frac{1}{2}u^2$), respectively, and τ_{ij}, q_x and q_y are the viscous stress tensor, the streamwise heat flux, and the wall-normal heat flux, respectively. To simplify Eq. (2), we follow Cebeci [28] to conduct the dimension analysis, and the details are reported in the Appendix. It is noted that Cebeci [28] and Younes [29] have already deduced the boundary-layer approximation of Eq. (2), thus we directly introduce it here. This simplified version takes the form of

$$\frac{\partial}{\partial y}(\bar{q}_y - \overline{\rho H''v''} + \overline{u\tau_{xy}}) = 0. \quad (3)$$

Integrating Eq. (3) along the whole boundary layer yields

$$\bar{q}_y - \overline{\rho H''v''} + \overline{u\tau_{xy}} = \bar{q}_w. \quad (4)$$

Considering the definition of H, its fluctuating component can be deduced as

$$H'' = c_p T'' + \frac{1}{2}u''^2 + \widetilde{u}u''. \quad (5)$$

Hence the second term on the left-hand side of Eq. (4) can be expanded as

$$\overline{\rho H''v''} = c_p\overline{\rho v''T''} + \overline{\rho\frac{1}{2}u''^2 v''} + \overline{\rho\widetilde{u}u''v''}, \quad (6)$$

and Eq. (4) can be recast as

$$\bar{q}_y - c_p\overline{\rho v''T''} = \bar{q}_w - \overline{u\tau_{xy}} + \overline{\rho\frac{1}{2}u''^2 v''} + \overline{\rho\widetilde{u}u''v''}. \quad (7)$$

Notably, the second term on the right-hand side of Eq. (6) is a third-order correlation, which can be conjectured to be smaller than the other two terms. In addition, the third term on the right-hand side of Eq. (6) can be approximated by its leading term,

$$\overline{\rho\widetilde{u}u''v''} \approx \widetilde{u}\overline{\rho u''v''}. \quad (8)$$

The last term on the left-hand side of Eq. (4) can also be approximated by its dominant term,

$$\overline{u\tau_{xy}} \approx \widetilde{u}\bar{\mu}\frac{d\widetilde{u}}{dy}, \quad (9)$$

where $\bar{\mu}$ denotes the mean dynamic viscosity. Accordingly, Eq. (7) can be rearranged as

$$\bar{q}_y - c_p \overline{\rho v'' T''} + \widetilde{u}\left(-\overline{\rho u'' v''} + \bar{\mu}\frac{d\widetilde{u}}{dy} \right) = \bar{q}_w. \tag{10}$$

We notice that the constant-stress layer approximation,

$$-\overline{\rho u'' v''} + \bar{\mu}\frac{d\widetilde{u}}{dy} = \overline{\tau}_w, \tag{11}$$

can be employed to further simplify the formula. $\overline{\tau}_w$ represents the mean wall shear stress. The constant-stress relationship is validated in the inner layer ($y/h \ll 1$) of high-Reynolds-number flows extensively, and frequently unitized for modeling purposes [9,28,30]. h denotes the channel half-height or the boundary layer thickness. It follows that Eq. (10) can be rewritten as

$$\bar{q}_y - c_p \overline{\rho v'' T''} = \bar{q}_w - \widetilde{u}\overline{\tau}_w. \tag{12}$$

To simplify the derivation, we further define the eddy thermal diffusivity as $\alpha_t = -\overline{\rho v'' \theta''}/(\frac{d\bar{\theta}}{dy})$ and the semilocal friction Reynolds number as $\mathrm{Re}_\tau^* = \mathrm{Re}_\tau \sqrt{(\bar{\rho}/\bar{\rho}_w)}/(\bar{\mu}/\bar{\mu}_w)$. Equation (12) can be rearranged as

$$\left(\frac{\alpha_t}{\bar{\mu}} + \frac{1}{\mathrm{Pr}}\right) \underbrace{\frac{h}{\mathrm{Re}_\tau^*}\sqrt{\bar{\rho}^+}\frac{d\bar{\theta}^+}{dy}}_{\psi_1} = 1 - \underbrace{\frac{\widetilde{u}\overline{\tau}_w}{\bar{q}_w}}_{\psi_2}. \tag{13}$$

ψ_2 is reported to be representative of the intensity of the aerodynamic heating [16] and ignored by Patel *et al.* [15] in their deduction [other terms are same as Eq. (13)], because they considered only the low-speed channel flows with the variable property. Under this condition, Patel *et al.* [15] pointed out that at a given Pr, ψ_1 is only a function of y^*, regardless of the flow property. In other words, $\psi_1(y^*)$ is a function which is independent of the flow property. It indicates that the function

$$\psi_3(y^*) = \frac{\alpha_t}{\bar{\mu}} + \frac{1}{\mathrm{Pr}} \tag{14}$$

is also independent of the flow property when Pr is given. To account for the aerodynamic-heating effects in high-speed flow, and maintain the invariant of $\psi_3(y^*)$ simultaneously, it can be directly conjectured that the function

$$\phi_{SL}(y^*) = \frac{\frac{h}{\mathrm{Re}_\tau^*}\sqrt{\bar{\rho}^+}\frac{d\bar{\theta}^+}{dy}}{1 - \frac{\widetilde{u}\overline{\tau}_w}{\bar{q}_w}} \tag{15}$$

is Mach number invariant. Integrating ϕ_{SL} with respect to y^* yields the semilocal-type transformation put forward by Chen *et al.* [17] recently (denoted as θ_{SL}^+ hereafter). Though the derivation of their transformation is different from that of the present study and also includes high-order terms. They claimed that this transformation can recover a compressible temperature profile to an incompressible one.

On the other hand, by analogy with the velocity transformation developed by van Driest [7], a similar Mach number invariant function can be built:

$$\phi_{VD}(y^+) = \frac{\sqrt{\bar{\rho}^+}\frac{d\bar{\theta}^+}{dy^+}}{1 - \frac{\widetilde{u}\overline{\tau}_w}{\bar{q}_w}}. \tag{16}$$

According to Eq. (13), it suggests that the function

$$\psi_4(y^+) = \left(\frac{\alpha_t}{\bar{\mu}} + \frac{1}{\mathrm{Pr}}\right)\frac{h}{\mathrm{Re}_\tau^*}\frac{dy^+}{dy} = \left(\frac{\alpha_t}{\bar{\mu}} + \frac{1}{\mathrm{Pr}}\right)\frac{\mathrm{Re}_\tau}{\mathrm{Re}_\tau^*} \tag{17}$$

is Mach invariant with respect to y^+ when Pr is given. Integrating ϕ_{VD} with respect to y^+ obtains another temperature transformation (denoted as θ_{VD}^+ hereafter), which is named the van Driest-type scaling by Chen *et al.* [17]. It is noted that ϕ_{VD} and ϕ_{SL} are considered as invariant functions for the whole inner layer by Chen *et al.* [17]. However, a detailed comparison has not been conducted.

When inspecting the invariants of ϕ_{SL} and ϕ_{VD} with the DNS database, we observe that they would be inaccurate in some cases (see the results shown in Sec. IV). It motivates us to look for other Mach number invariant functions. To construct an invariant function for the mean temperature field, it should be emphasized that several constraints and experience ought to be obeyed and followed. First, the van Driest-type differentiation, $\sqrt{\bar{\rho}^+}d\bar{\theta}^+$ (for mean velocity, that is $\sqrt{\bar{\rho}^+}d\bar{u}^+$), should be kept to account for the density variation; second, the semilocal scaling should be utilized to diminish the Mach number effects in the inner layer, which has been demonstrated extensively in previous studies [9,12,31]; third, the term ψ_2 should be included in the function to elucidate the aerodynamic-heating effects. It manifests as the inclusion of ψ_2 in the denominators of Eq. (15) and Eq. (16). Based on the above understanding, we hypothesize that a function,

$$\phi_S(y^*) = \frac{\sqrt{\bar{\rho}^+}\frac{d\bar{\theta}^+}{dy^*}}{1 - \frac{\tilde{u}\tilde{\tau}_w}{\bar{q}_w}}, \tag{18}$$

is Mach number invariant with respect to y^* in the log region. If this is true, it implies that the function

$$\psi_5(y^*) = \left(\frac{\alpha_t}{\bar{\mu}} + \frac{1}{\text{Pr}}\right)\frac{h}{\text{Re}_\tau^*}\frac{dy^*}{dy} = \left(\frac{\alpha_t}{\bar{\mu}} + \frac{1}{\text{Pr}}\right)\left(1 + \frac{y}{\text{Re}_\tau^*}\frac{d\text{Re}_\tau^*}{dy}\right) \tag{19}$$

is Mach invariant with respect to y^* when Pr is given. We notice that Younes and Hickey [14] reported the Mach number invariant of $\sqrt{\bar{\rho}^+}du^+/dy^*$ in the log layer very recently. They pointed out that this function denotes a semilocal normalized mean spanwise vorticity, which can account for the property variations in the log region. Considering the similarities between the velocity and temperature fields [1,32–35], it is reasonable to hypothesize that ϕ_S, which also accounts for the aerodynamic-heating effects, is a Mach number invariant function for the mean temperature field in the log region.

It should be noted that the original formulas of ϕ_{VD}, ϕ_{SL}, and ϕ_S are singular for an adiabatic wall because θ^+ cannot be mathematically defined. This problem can be overcome by expanding the definition of θ_τ. In this way, their alternative formulas can be given as

$$\phi_{SL}(y^*) = \frac{\sqrt{\bar{\rho}^+}\bar{\rho}_w c_p u_\tau}{\bar{q}_w - \tilde{u}\tilde{\tau}_w}\frac{h}{\text{Re}_\tau^*}\frac{d\bar{\theta}}{dy}, \tag{20}$$

$$\phi_{VD}(y^+) = \frac{\sqrt{\bar{\rho}^+}\bar{\rho}_w c_p u_\tau}{\bar{q}_w - \tilde{u}\tilde{\tau}_w}\frac{d\bar{\theta}}{dy^+}, \tag{21}$$

$$\phi_S(y^*) = \frac{\sqrt{\bar{\rho}^+}\bar{\rho}_w c_p u_\tau}{\bar{q}_w - \tilde{u}\tilde{\tau}_w}\frac{d\bar{\theta}}{dy^*}, \tag{22}$$

where θ_τ is not involved.

Let us summarize the assumptions and hypotheses related to the above discussion. They are listed as follows:

(1) The constant-stress layer approximation (11)

(2) The neglect of the high-order terms when deducing Eq. (8), Eq. (9), and Eq. (10)

(3) The invariants of the functions ψ_3, ψ_4, and ψ_5.

The first approximation has been validated extensively, as we mentioned above. As a sanity check, we define the function

$$\Pi_1 = \frac{-\overline{\rho u''v''} + \bar{\mu}\frac{d\tilde{u}}{dy}}{\bar{\tau}_w} \tag{23}$$

to verify it. $\Pi_1 \approx 1$ in the inner layer indicates the validation of this simplification. We can assess the validation of Eq. (12) within the inner layer to justify the second assumption indirectly. To this end, we define the function

$$\Pi_2 = \frac{\overline{q}_w - \widetilde{u}\overline{\tau}_w}{\overline{q}_y - c_p \overline{\rho v'' T''}}. \tag{24}$$

If $\Pi_2 \approx 1$ in the inner layer, it suggests that the second assumption is acceptable. Moreover, Eq. (9) can be directly examined for some cases, because several open-source data contain the related statistics. Hence, we define the function

$$\Pi_3 = \frac{\widetilde{u}\overline{\mu}\frac{d\widetilde{u}}{dy}}{\overline{u\tau_{xy}}}. \tag{25}$$

For the third hypothesis, we will also appraise it in the next section. It should be acknowledged that the invariants of these specific functions can not be justified mathematically for now. Hence, in the present study, we decide to do it in a heuristic way by exploiting the DNS database extensively. Such a model of research is consistent with those of Patel *et al.* [10] and Patel *et al.* [15], who put forward the semilocal-type transformations for the mean velocity and scalar fields in low-speed channel flows with variable property successfully.

Finally, it is worth noting that the ignoring of the high-order terms is observed to bear non-negligible effects on the accuracy of the deduced scalings for some cases; see Sec. III. In light of this, it is necessary to give the complete form of the governing equation of the mean temperature for comparison:

$$\left(\frac{\alpha_t}{\overline{\mu}} + \frac{1}{\text{Pr}}\right)\frac{h}{\text{Re}_\tau^*}\sqrt{\overline{\rho}^+}\frac{d\overline{\theta}^+}{dy} = 1 - \frac{\psi_6}{\overline{q}_w}, \tag{26}$$

where

$$\psi_6 = \overline{u\tau_{xy}} - \overline{\rho\frac{1}{2}u''^2 v''} - \overline{\rho\widetilde{u}u''v''}. \tag{27}$$

In Eq. (13), ψ_6 is modeled as $\widetilde{u}\overline{\tau}_w$. If the third assumption above is valid, the modified versions of ϕ_{SL}, ϕ_{VD}, and ϕ_S read as

$$\phi_{SL,m}(y^*) = \frac{\frac{h}{\text{Re}_\tau^*}\sqrt{\overline{\rho}^+}\frac{d\overline{\theta}^+}{dy}}{1 - \frac{\psi_6}{\overline{q}_w}}, \tag{28}$$

$$\phi_{VD,m}(y^+) = \frac{\sqrt{\overline{\rho}^+}\frac{d\overline{\theta}^+}{dy^+}}{1 - \frac{\psi_6}{\overline{q}_w}}, \tag{29}$$

$$\phi_{S,m}(y^*) = \frac{\sqrt{\overline{\rho}^+}\frac{d\overline{\theta}^+}{dy^*}}{1 - \frac{\psi_6}{\overline{q}_w}}. \tag{30}$$

The corresponding temperature transformations $(\theta_{SL,m}^+, \theta_{VD,m}^+, \theta_{S,m}^+)$ can also be defined and not shown here for brevity. We will appraise the results of the simplification Eq. (13) by comparing with those of Eq. (26) frequently, and ascertain the terms that cannot be ignored or modeled.

III. DATA DESCRIPTION AND ASSUMPTIONS VERIFICATION

In this section, we will briefly introduce the open-source DNS database used in the present study to appraise the three Mach number invariant functions of the mean temperature field mentioned above and verify the associated assumptions in Sec. II. All these simulations are carried out with a constant Pr within 0.7 to 0.72. The mean temperature statistics obtained in an incompressible
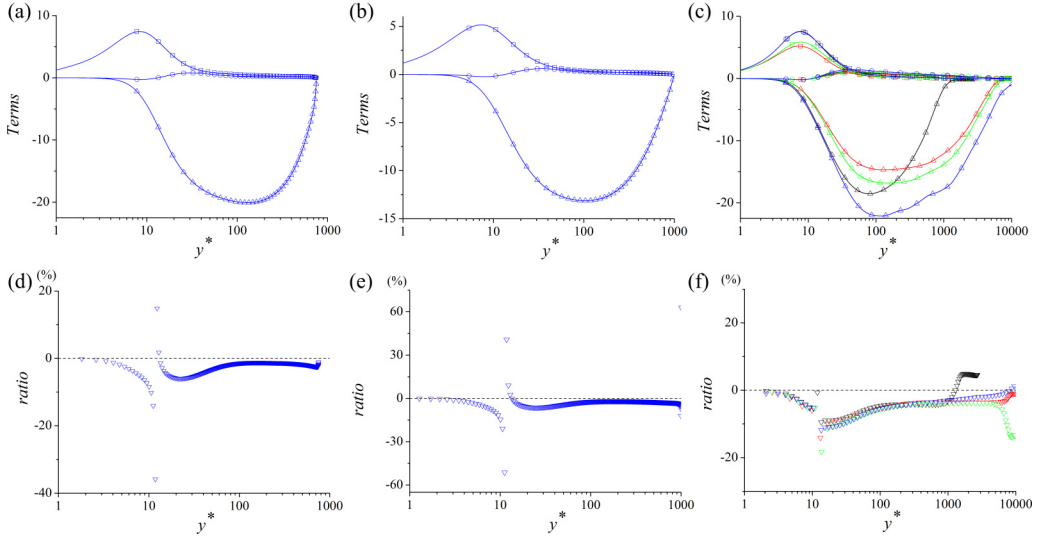
FIG. 1. (a)–(c) Distributions of □: $\overline{u\tau_{xy}}^+$; ○: $\overline{\rho\frac{1}{2}u''^2v''}^+$; △: $\overline{\rho\widetilde{u}u''v''}^+$ in a compressible turbulent channel flow with (a) isothermal, (b) adiabatic walls, and (c) supersonic/hypersonic turbulent boundary layers with cold walls [18,37]; (d)–(f) distributions of the ratio between $\overline{\rho\frac{1}{2}u''^2v''}^+$ and the sum of $\overline{u\tau_{xy}}^+$ and $\overline{\rho\widetilde{u}u''v''}^+$ in a compressible turbulent channel flow with (d) isothermal, (e) adiabatic walls, and (f) supersonic/hypersonic turbulent boundary layers with cold walls. The core Mach number of the channel is 2.0. In panels (c) and (f) each case is represented by a curve with a particular color.

channel flow with $\mathrm{Re}_\tau = 5000$ and $\mathrm{Pr} = 0.71$ [36] are used for reference. $\widetilde{u}$ and $\overline{\rho u''v''}$ are not provided by some data, and we will adopt the existing $\bar{u}$ and $\overline{\rho u'v'}$ instead. In the present study, the results of the DNS database are represented by blue lines in the figures if not specified otherwise.

The first type of data is from Lusher and Coleman [37], where the compressible turbulent channel flows with mixed thermal conditions are simulated (seven cases). The lower walls are isothermal, and the upper ones are adiabatic. The data cover a wide range of Reynolds numbers with maximal Mach numbers between 1.1 and 2.2, and a constant $\mathrm{Pr} = 0.7$. The flows over two sides can be investigated separately to elucidate the effects of the isothermal and adiabatic wall conditions. The detailed computational setups and the numerical methods can be found in Lusher and Coleman [37]. The statistics of this data set are ample, which are suitable for the verification of the hypotheses put forward in Sec. II.

The second type of flow considered here is the supersonic/hypersonic turbulent boundary layers with extensive Mach numbers and wall temperatures. The data are taken from Zhang $et\ al.$ [18] and Cogo $et\ al.$ [38], with Mach number and wall-to-recovery temperature ranging from 2 to 14, and 0.76 to 0.18, respectively. These cases contain eight cold walls with nonmonotonic temperature distributions and heat transfer, which provide an excellent platform for examining the Mach number invariants of these specific functions. Especially, the data of Zhang $et\ al.$ [18] (four cases with cold walls) contain rich information. We will appeal to them to verify the assumptions.

First, we compare the magnitude of each term in the right-hand side of Eq. (6) in Fig. 1 to demonstrate that ignoring the correlation term $\overline{\rho\frac{1}{2}u''^2v''}$ is convincing, as only this term is ignored and not modeled. For the flows over both isothermal and adiabatic walls, the case with the highest Re_τ^* in the database of Lusher and Coleman [37] is chosen, and the approximation Eq. (8) is used to estimate $\overline{\rho\widetilde{u}u''v''}$. Results are shown in Figs. 1(a) and 1(b). As can be seen, $\overline{u\tau_{xy}}$ is dominant in magnitude in the near-wall region, whereas $\overline{\rho\widetilde{u}u''v''}$ is dominant in the log region. By contrast, the magnitudes of $\overline{\rho\frac{1}{2}u''^2v''}$ are negligible. It suggests that for these two types of flows, the ignoring
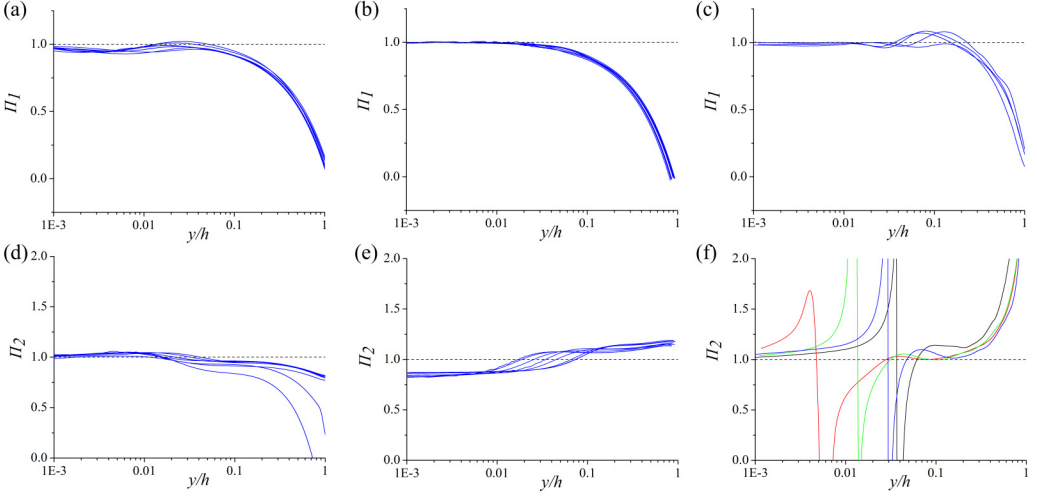
FIG. 2. (a)–(c) Distributions of Π_1 in turbulent channel flows with (a) isothermal walls [37], (b) adiabatic walls [37], and (c) supersonic/hypersonic turbulent boundary layers with cold walls [18]; (d)–(f) distributions of Π_2 in turbulent channel flows with (d) isothermal walls [37], (e) adiabatic walls [37], and (f) supersonic/hypersonic turbulent boundary layers with cold walls [18]. In panel (f) each case is represented by a curve with a particular color.

of the three-order correlation $\overline{\rho \frac{1}{2} u''^2 v''}$ is plausible in these two regions. As a result, $\psi_6 \approx \overline{u \tau_{xy}} - \overline{\rho \tilde{u} u'' v''} \approx \overline{u \tau_{xy}} - \tilde{u} \overline{\rho u'' v''}$ is well established. For supersonic/hypersonic turbulent boundary layers, the scenario is similar; see Fig. 1(c). It should be noted that we use $\overline{u'' \tau_{xy}''} + \bar{u} \overline{\tau_{xy}}$ to approximate $\overline{u \tau_{xy}}$ for this kind of flow, due to the lack of the statistics of $\overline{u \tau_{xy}}$ in the database of Zhang *et al.* [18]. In short, for the three types of flows under consideration, the three-order correlation term $\overline{\rho \frac{1}{2} u''^2 v''}$ can be ignored by and large. To show this point more clearly, Figs. 1(d)–1(f) display the variations of the ratios between $\overline{\rho \frac{1}{2} u''^2 v''}^+$ and the sum of $\overline{u \tau_{xy}}^+$ and $\overline{\rho \tilde{u} u'' v''}^+$ for these three types of flows. One can see that, for each type of flow, the ratio varies abruptly only around $y^* = 11$, that is, the buffer region. It indicates that the three-order correlation is only non-negligible in this small range. In fact, the results shown in Fig. 12 and Fig. 13 below imply that as long as the accuracies of the Mach number invariants of the temperature gradient functions in the viscous sublayer and the log region are settled, the derived transformation is sufficiently accurate. After all, the transformation is an integral expression, and its effectiveness is dependent on the overall Mach number invariants of the temperature gradient functions. Hence, we choose to ignore this term.

The constant-stress layer approximation is then examined in Figs. 2(a)–2(c), which display the distributions of Π_1 in turbulent channel flows with (a) isothermal and (b) adiabatic walls [37], and (c) supersonic/hypersonic turbulent boundary layers with cold walls [18]. It can be seen that for these three different types of flows, $\Pi_1 \approx 1$ is preserved in the inner layer ($y/h < 0.1$), and the deviations are typically $\leqslant 12\%$. It demonstrates that invoking the constant-stress layer approximation for the simplification of Eq. (10) is acceptable. Figures 2(d)–2(f) show the variations of Π_2 as functions of wall-normal height to check indirectly whether the neglect of the high-order terms is reasonable. For turbulent channel flows with (d) isothermal and (e) adiabatic walls, $\Pi_2 \approx 1$ in the whole inner layer, with a maximum error smaller than 15%. However, the deviations of Π_2 from 1 are more significant for flows over adiabatic walls in the near-wall region. For supersonic/hypersonic turbulent boundary layers with cold walls, the profiles of Π_2 vary sharply around the extreme points of the mean temperature profiles (denoted as y_c hereafter). It indicates that these assumptions fail near y_c. However, apart from the wall-normal zone adjacent to y_c, $\Pi_2 \approx 1$ is validated in the other
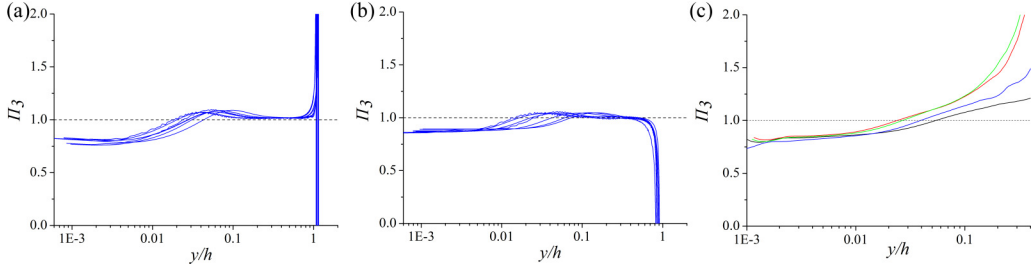
FIG. 3. Distributions of Π_3 in turbulent channel flows with (a) isothermal, (b) adiabatic walls, and (c) supersonic/hypersonic turbulent boundary layers with cold walls [18,37]. In panel (c) each case is represented by a curve with a particular color.

regions within the inner layer. However, some deviations can still be observed in the near-wall region and the log region. Figures 3(a)–3(c) display the distributions of Π_3 in turbulent channel flows with (a) isothermal, (b) adiabatic walls, and (c) supersonic/hypersonic turbulent boundary layers with cold walls [18,37]. It can be seen that for these three types of flows, the maximum deviations of Π_3 from 1 occur in the vicinity of the wall, where the influences of compressibility are remarkable. It may underline the fact that the deviations of Π_2 from 1 shown in Figs. 2(e) and 2(f) are result from the error in simplification Eq. (9). The ignored high-order terms during this simplification take effect in the establishment of Eq. (13) in the inner layer.

To further quantify the errors in simplification Eq. (9), a modified version of the test function Π_2 can be defined as

$$\Pi_{2,m} = \frac{\overline{q}_w - \psi_6}{\overline{q}_y - c_p \overline{\rho v'' T''}}. \tag{31}$$

It can be seen that $\widetilde{u}\overline{\tau}_w$ in the definition of Π_2 is replaced by $\psi_6 \approx \overline{u\tau_{xy}} - \overline{\rho\widetilde{u}u''v''}$ in that of $\Pi_{2,m}$. Figures 4(a)–4(c) display the distributions of $\Pi_{2,m}$ in turbulent channel flows with (a) isothermal, (b) adiabatic walls, and (c) supersonic/hypersonic turbulent boundary layers with cold walls by using the same data as in Figs. 2(d)–2(f) and Figs. 3(a)–3(c). Surprisingly, the errors in the inner region ($y/h < 0.1$) are remarkably attenuated for turbulent channel flows with adiabatic walls. The maximum deviation of $\Pi_{2,m}$ from 1 is less than 5% for this type of flow in the inner region. For turbulent channel flows with isothermal walls, the improvements are not significant. It suggests that for channel flows with isothermal walls, Eq. (13) is sufficiently accurate, while for turbulent channel flows with adiabatic walls, it is not. For supersonic/hypersonic turbulent boundary layers with cold walls, the errors in the near-wall region also reduced, compared with the results exhibited in Fig. 2(f). All these observations indicate that the errors of Eq. (13) in the near-wall region
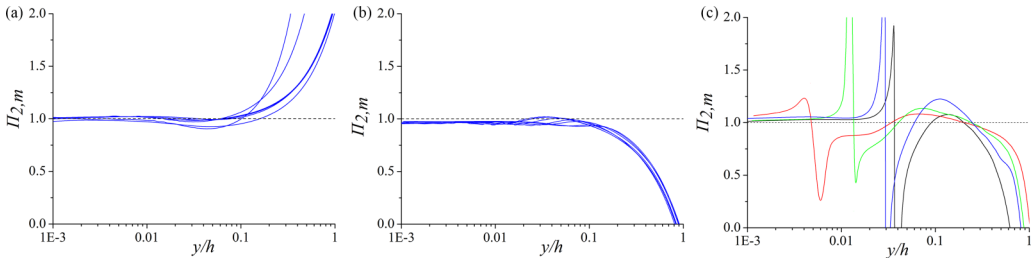

FIG. 4. Distributions of $\Pi_{2,m}$ in turbulent channel flows with (a) isothermal and (b) adiabatic walls and (c) supersonic/hypersonic turbulent boundary layers with cold walls [18,37]. In panel (c) each case is represented by a curve with a particular color.
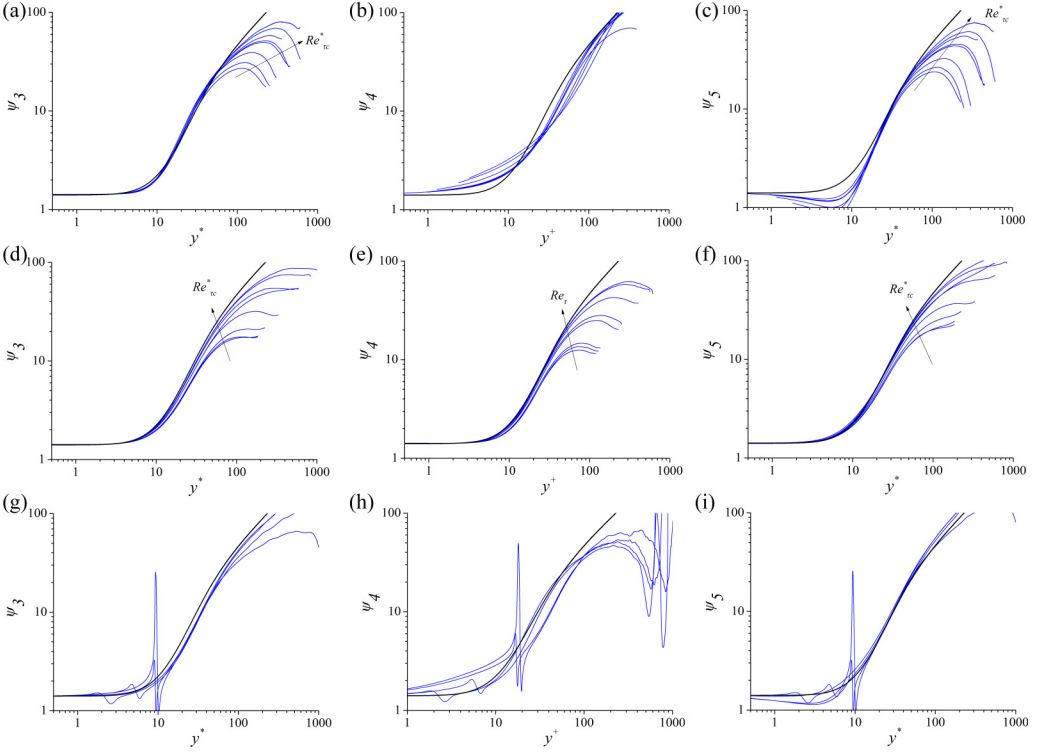
FIG. 5. (a)–(c) Distributions of (a) ψ_3, (b) ψ_4, and (c) ψ_5 in turbulent channel flows with isothermal walls [37]; (d)–(f) distributions of (d) ψ_3, (e) ψ_4, and (f) ψ_5 in turbulent channel flows with adiabatic walls [37]; (g)–(i) distributions of (g) ψ_3, (h) ψ_4, and (i) ψ_5 in supersonic/hypersonic turbulent boundary layers with cold walls [18]. Incompressible channel data of Alcántara-Ávila *et al.* [36] is shown for reference (black lines).

should be mainly ascribed to the simplification (9), $\overline{u\tau_{xy}} \approx \widetilde{u}\bar{\mu}\frac{d\widetilde{u}}{dy}$. Furthermore, current analyses also demonstrate that the simplification (8), $\overline{\rho\widetilde{u}u''v''} \approx \widetilde{u}\overline{\rho u''v''}$, is acceptable for all these three types of flows.

Finally, we assess the Mach number invariants of ψ_3, ψ_4, and ψ_5 in different types of flows. Figures 5(a)–5(c) show the distributions of ψ_3, ψ_4, and ψ_5 in turbulent channel flows with isothermal walls [37], respectively. ψ_4 of each case deviates from the reference data visibly, whereas ψ_3 and ψ_5 show reasonable collapses with the incompressible data in the log layer. It signifies that for turbulent channel flows with isothermal walls, ϕ_{SL} ($\phi_{SL,m}$) and ϕ_S ($\phi_{S,m}$) may be the Mach number invariant functions in the log layer. Which one is better remains to be checked in Sec. IV. For the viscous sublayer, only the distributions of ψ_3 collapse with the reference one. The counterparts of turbulent channel flows with adiabatic walls [37] are compared in Figs. 5(d)–5(f). It is not difficult to observe that the variations of ψ_5 are most consistent with that of the reference data in the log region. For the viscous sublayer, no discernible difference among them can be observed. It verifies the applicability of the scaling proposed by the present study for this kind of flow. Figures 5(g)–5(i) exhibit the distributions of ψ_3, ψ_4, and ψ_5 in supersonic/hypersonic turbulent boundary layers with cold walls [18], respectively. The humps around $y^+ (y^*) \approx 10$–20 in the panels result from the nonmonotonicity of the mean temperature profiles. The performances of these three functions are utterly distinct. For both ψ_3 and ψ_4, they deviate from the reference data evidently within $20 \leqslant y^+ (y^*) \leqslant 100$, whereas for ψ_5, good collapses are obtained in this range. It indicates that the scaling ϕ_S ($\phi_{S,m}$) is superior to
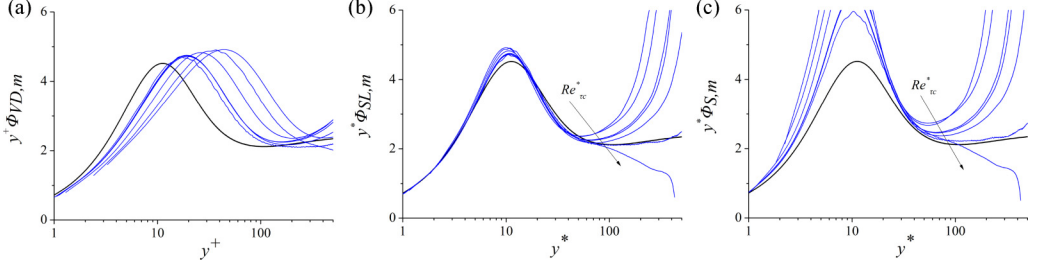
FIG. 6. Distributions of (a) $y^+\phi_{VD,m}$, (b) $y^*\phi_{SL,m}$, and (c) $y^*\phi_{S,m}$ in the isothermal sides of turbulent channel flows with mixed thermal conditions [37] (seven cases). All cases are of monotonic temperature distributions. Incompressible channel data of Alcántara-Ávila *et al.* [36] with $\mathrm{Re}_\tau = 5000$ and $\mathrm{Pr} = 0.71$ are shown for reference (black lines).

the other two functions for supersonic/hypersonic turbulent boundary layers with cold walls in the log region.

In summary, analyses conducted in this section demonstrate that the assumptions and hypotheses raised in Sec. II are roughly valid in the inner region for all three types of flows under consideration. However, the simplification Eq. (9) is not entirely accurate for the near-wall regions of flows over adiabatic walls and supersonic/hypersonic turbulent boundary layers with cold walls. Furthermore, the Mach number invariant of ψ_5 is compared with those of ψ_3 and ψ_4. It is worth noting again that the Mach number invariants of ψ_3, ψ_4, and ψ_5 are closely connected with the properties of the temperature gradient functions ϕ_{SL} ($\phi_{SL,m}$), ϕ_{VD} ($\phi_{VD,m}$), and ϕ_S ($\phi_{S,m}$), respectively. Hence, we will directly appraise these temperature gradient functions in Sec. IV. To quantify the errors of these functions, the integrated error of a temperature gradient function can be defined as

$$\epsilon = \frac{\int_\alpha^\beta |\phi_a - \phi_I| dy_a}{\int_\alpha^\beta \phi_I dy_a}, \tag{32}$$

where ϕ_a is the temperature gradient function, y_a is the nondimensional wall-normal coordinate that corresponds to a specific gradient function, α and β are the bounds of the integration, and ϕ_I denotes the incompressible reference gradient profile (normalized with respect to wall units) for a channel flow at $\mathrm{Re}_\tau = 5000$ [36]. In the following sections, for channel flows with isothermal and adiabatic walls, we show only the results associated with $\theta_{SL,m}^+$, $\theta_{VD,m}^+$, and $\theta_{S,m}^+$. The reason is given above. For the database of Cogo *et al.* [38] of supersonic/hypersonic turbulent boundary layers with cold walls, we show the results related to θ_{SL}^+, θ_{VD}^+, and θ_S^+ due to the lack of the statistics of $\overline{u\tau_{xy}}$ in the open-source database, whereas for the database of Zhang *et al.* [18], we exhibit the results related to $\theta_{SL,m}^+$, $\theta_{VD,m}^+$, and $\theta_{S,m}^+$.

IV. ASSESSMENT OF MACH NUMBER INVARIANTS OF THE TEMPERATURE GRADIENT FUNCTIONS

A. Compressible turbulent channel flows with isothermal walls

Figures 6(a)–6(c) show the distributions of $y^+\phi_{VD,m}$, $y^*\phi_{SL,m}$, and $y^*\phi_{S,m}$ in compressible channel flows with isothermal walls [37], respectively. By careful comparison, it can be found that only $\phi_{SL,m}$ is a Mach number invariant function in the viscous sublayer ($y^* < 5$), whereas $\phi_{VD,m}$ and $\phi_{S,m}$ deviate from the reference data remarkably. For the lower part of the log region, $20 < y^* < 40$, $\phi_{S,m}$ and $\phi_{SL,m}$ behave similarly and are roughly close to the incompressible profile, whereas the distributions of $\phi_{VD,m}$ are case-dependent. In Fig. 7 the integrated errors of these functions in the log region are compared with $\alpha = 20$ and $\beta = 40$. The errors of $\phi_{SL,m}$ and $\phi_{S,m}$ are very close to each other in the log region, and significantly lower than those of $\phi_{VD,m}$. All in all, $\phi_{SL,m}$ performs
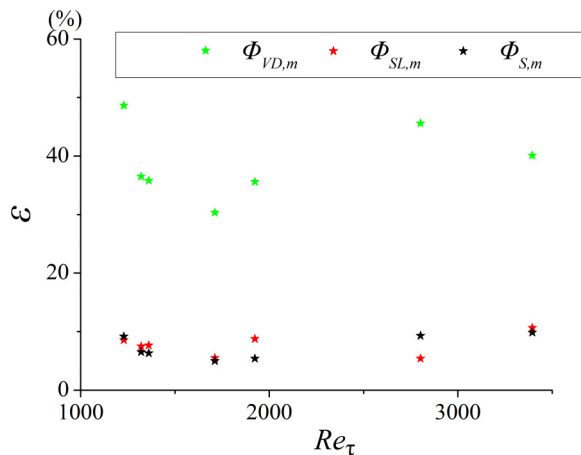
FIG. 7. Integrated errors of $\phi_{VD,m}$, $\phi_{SL,m}$, and $\phi_{S,m}$ with respect to Re_τ in the log region for isothermal sides of turbulent channel flows with mixed thermal conditions [37].

the best in the whole inner layer of this type of flow, $\phi_{VD,m}$ the worst, and the performance of $\phi_{S,m}$ is as good as that of $\phi_{SL,m}$ in the log region.

B. Compressible turbulent channel flows with adiabatic walls

We concentrate on the seven cases with adiabatic walls in Lusher and Coleman [37] (without heat transfer, monotonic temperature distributions) herein. The variations of $y^+\phi_{VD,m}$, $y^*\phi_{SL,m}$, and $y^*\phi_{S,m}$ with respect to y^+ or y^* for the adiabatic sides are shown in Figs. 8(a)–8(c), respectively. At first glance, all these functions work well in the inner layer. As the increases of the Reynolds number, their profiles tend to overlap with that of the reference data. If we look closely and and quantify the errors of these three functions (see Fig. 9), the performance of $\phi_{S,m}$ can be observed to be superior to those of $\phi_{SL,m}$ and $\phi_{VD,m}$ for all cases in both the viscous sublayer and the log region, and its error in the log region is decreased as the increase of the Reynolds number. These observations suggest that $\phi_{S,m}$ can be treated as an invariant function in the inner layer of turbulent channel flows with adiabatic walls indeed. For the calculation of the integrated errors in the viscous sublayer, α and β are chosen as 0 and 5, respectively. For the log region, they are set as 20 and 60, respectively.
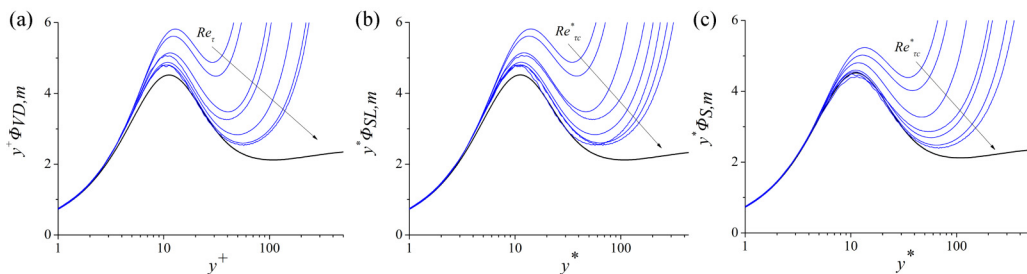

FIG. 8. Distributions of (a) $y^+\phi_{VD,m}$, (b) $y^*\phi_{SL,m}$, and (c) $y^*\phi_{S,m}$ in compressible channel flows with adiabatic walls (without heat transfer) and monotonic temperature distributions [37].
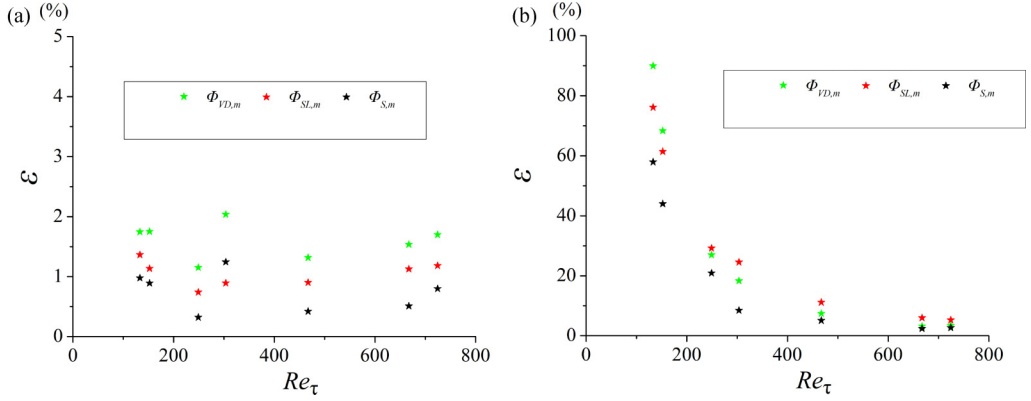
FIG. 9. Integrated errors of $\phi_{VD,m}$, $\phi_{SL,m}$, and $\phi_{S,m}$ with respect to Re_τ in the (a) viscous sublayer and the (b) log region for compressible turbulent channel flows with adiabatic walls [37].

C. Supersonic/hypersonic turbulent boundary layers with cold walls

Figure 10 shows the distributions of $y^+\phi_{VD}$ ($y^+\phi_{VD,m}$), $y^*\phi_{SL}$ ($y^*\phi_{SL,m}$), and $y^*\phi_S$ ($y^*\phi_{S,m}$) in the [Figs. 10(a)–10(c)] viscous sublayer (four cases) and the [Figs. 10(d)–10(f)] log region (seven cases). Due to the nonmonotonicity of the mean temperature profiles in wall turbulence with cold walls, we remove the cases with y_c adjacent to the viscous sublayer in Figs. 10(a)–10(c) and the log region in Figs. 10(d)–10(f), because in the vicinity of the extreme points, some assumptions for the deduction of the invariant functions are invalid [see Fig. 2(f)], and thus the magnitudes of them alter sharply.

For ϕ_{VD} ($\phi_{VD,m}$), the results are most case-dependent and sensitive to the Mach number and the wall thermal condition, regardless of the wall-normal location. For ϕ_{SL} ($\phi_{SL,m}$), its profiles are
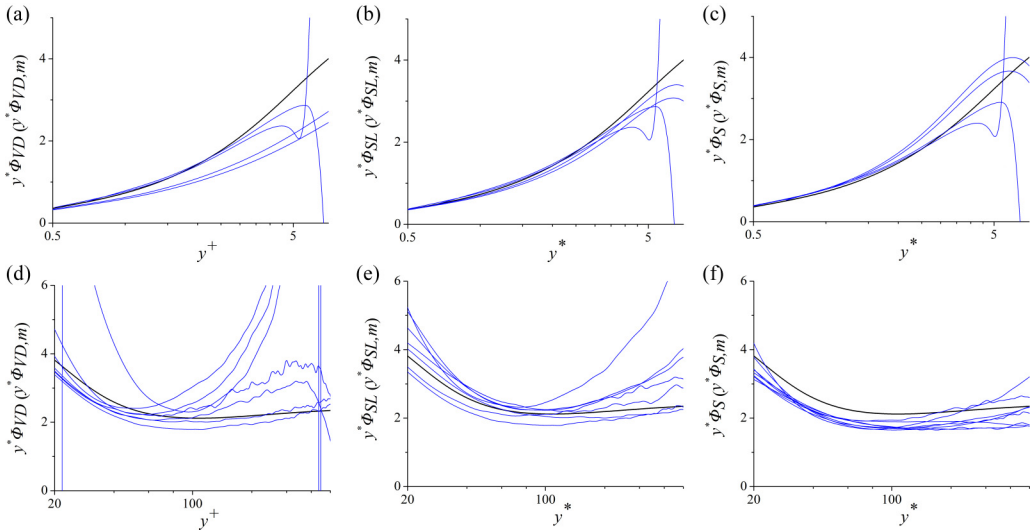

FIG. 10. Distributions of $y^+\phi_{VD}$ ($y^+\phi_{VD,m}$), $y^*\phi_{SL}$ ($y^*\phi_{SL,m}$), and $y^*\phi_S$ ($y^*\phi_{S,m}$) in the (a)–(c) viscous sublayer (four cases) and the (d)–(f) log region (seven cases) of supersonic/hypersonic turbulent boundary layers [18,38]. These cases include cold walls with nonmonotonic distributions with heat transfer. Black lines are the same as Fig. 6.
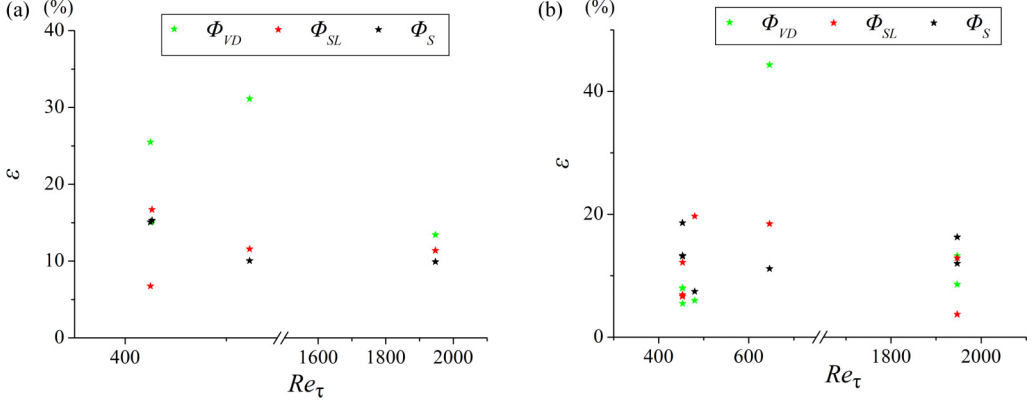
FIG. 11. Integrated errors of ϕ_{VD} ($\phi_{VD,m}$), ϕ_{SL} ($\phi_{SL,m}$), and ϕ_S ($\phi_{S,m}$) with respect to Re_τ in (a) the viscous sublayer and (b) the log region of supersonic/hypersonic turbulent boundary layers with cold walls [18,38].

roughly consistent with the reference data in the viscous sublayer and deviate from it in the log region. The profiles of ϕ_S ($\phi_{S,m}$) of all cases collapse well in the inner region. Figures 11(a) and 11(b) gauge the integrated errors of these three functions in the viscous sublayer ($\alpha = 0$, $\beta = 5$) and the log region ($\alpha = 30$, $\beta = 80$), respectively. It is transparent that the errors of ϕ_S and ϕ_{SL} are at a similar level in the viscous sublayer. In the log region, the errors of ϕ_S are also stable and small. It is noted that in some cases, the errors of ϕ_S are larger than those of ϕ_{SL} and ϕ_{VD}. This is not strange, because the distributions of ϕ_{SL} and ϕ_{VD} are more spread than those of ϕ_S [see Figs. 10(d)–10(f)]. Finally, it is worth noting that the viscous sublayers of several cases ($y_c^* = 0$–5) considered here are not far from the extreme point of the temperature profiles ($y_c^* \approx 9$). As a result, the validation of Mach number invariants of the scalings in this region would be inevitably impacted by the invalidation of the governing Eqs. (13) and (26) near y_c. In light of this, choosing ϕ_{SL} ($\phi_{SL,m}$) or ϕ_S ($\phi_{S,m}$) as the Mach number invariant function in the viscous sublayer of this type of flow is only a makeshift choice. Further work should be done on the relationship between the high-order terms and the mean temperature profile in the viscous sublayer and the buffer layer. On the other hand, for the log region far from the extreme point, the superiority of $\phi_{S,m}$ over $\phi_{VD,m}$ and $\phi_{SL,m}$ as a Mach number invariant function is well established; see Fig. 10. The Mach number invariant functions of mean temperature field presented case by case above are summarized in Table I.

V. TEMPERATURE TRANSFORMATION

To develop an advanced modeling approach, it is essential to derive a temperature transformation to recover the mean temperature profiles in compressible wall turbulence with various Mach numbers and wall thermal conditions into the classical incompressible ones. Upon the above discussion, for the flows over isothermal walls, it is not difficult to observe that the most effective way is to deploy $\phi_{SL,m}$ in the whole inner region, $\theta_{SL,m}^+(y^*) = \int \phi_{SL,m} \, dy^*$. For compressible channel flows with adiabatic walls and supersonic/hypersonic turbulent boundary layers with cold walls, the appropriate transformations are $\theta_{S,m}^+(y^*) = \int \phi_{S,m} \, dy^*$ ($\theta_S^+(y^*) = \int \phi_S \, dy^*$). For those flows above

TABLE I. Mach number invariant functions of mean temperature field in different zones of each type of flow.

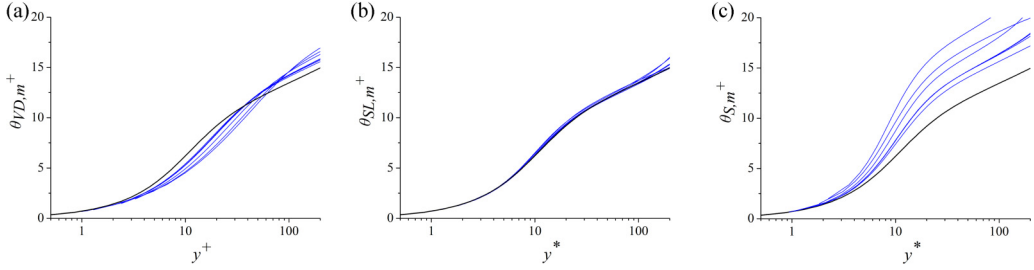| Region	Isothermal channel	Adiabatic channel	Cold boundary layer
Viscous sublayer	$\phi_{SL,m}$	$\phi_{S,m}$	$\phi_{SL,m}, \phi_{S,m}$
Log region	$\phi_{SL,m}, \phi_{S,m}$	$\phi_{S,m}$	$\phi_{S,m}$

FIG. 12. Temperature profiles transformed as per the (a) van Driest-type, (b) semilocal-type, and (c) present $\phi_{S,m}$-based-type transformations for the isothermal sides of turbulent channel flows with mixed thermal conditions [37]. Incompressible temperature profile of Alcántara-Ávila *et al.* [36] is shown for reference (black lines).

the cold walls with nonmonotonic temperature profiles, if y_c^* is located in the buffer layer, $\phi_{S,m}$ (ϕ_S) works well in the viscous sublayer and the log region. Hence, for this circumstance, $\theta_{S,m}^+$ (θ_S^+) can recover the variation tendencies of the incompressible profiles in these two regions, i.e., the slope of the corresponding incompressible one.

Figures 12(a), 12(b), and 12(c) show the transformed mean temperature velocity profiles by employing the functions $\phi_{VD,m}$, $\phi_{SL,m}$, and $\phi_{S,m}$ for the compressible channel flows with isothermal walls [37], respectively. It can be seen that the profiles of $\theta_{VD,m}^+$ and $\theta_{S,m}^+$ are not consistent with the incompressible one in the inner layer, whereas $\theta_{SL,m}^+$ can recover the incompressible counterparts in the inner layer perfectly.

Figures 13(a), 13(b), and 13(c) display the results of $\theta_{VD,m}^+$, $\theta_{SL,m}^+$, and $\theta_{S,m}^+$ for the adiabatic sides of compressible turbulent channel flows with mixed thermal conditions [37], respectively. It is not difficult to observe that the performance of $\theta_{S,m}^+$ is the best, and their slopes most closely match the incompressible one. The slight advantage of $\phi_{S,m}$ over $\phi_{VD,m}$ and $\phi_{SL,m}$ in the inner layer (see Fig. 9) leads to the collapses of the profiles with the incompressible one for high-Reynolds-number cases. Note that a paper published very recently by Huang *et al.* [39] also displayed the transformed profiles of compressible channel flows with adiabatic walls by leveraging the semilocal-type scaling and using the same database; see Fig. 11(b) of their paper. Even in high Reynolds numbers, the transformed profiles reported in their study do not match well the reference data in both the viscous sublayer and the log region. Specifically, the magnitude of the transformed profile of each case is slightly larger than that of the reference in the viscous sublayer and the log region. The present study improves their results through clarifying the role of the high-order terms and deploying an alternative Mach number invariant function, $\phi_{S,m}$.
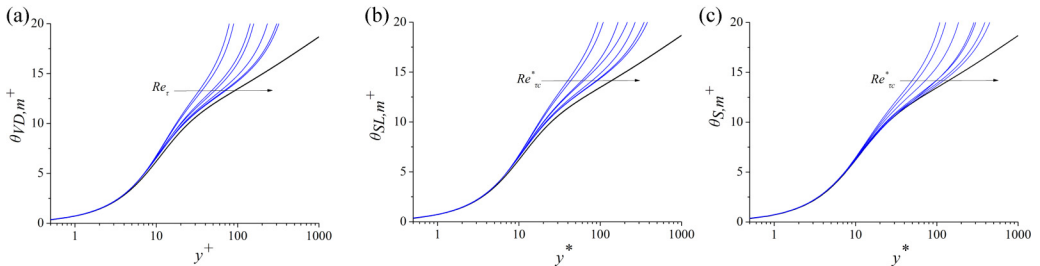

FIG. 13. Temperature profiles transformed as per the (a) van Driest-type, (b) semilocal-type, and (c) $\phi_{S,m}$-based type transformations for the compressible channel flows with adiabatic walls [37]. Black lines are the same as Fig. 12.
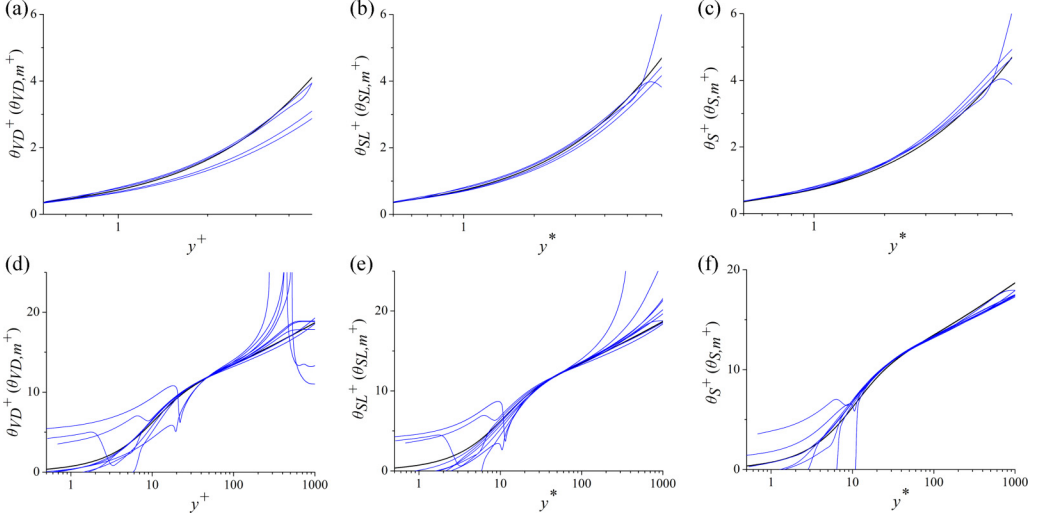
FIG. 14. Temperature profiles transformed as per the (a) van Driest-type, (b) semilocal-type, and (c) present $\phi_S(\phi_{S,m})$-based-type transformations for supersonic/hypersonic turbulent boundary layers (namely, the cases shown in Fig. 10) [18,38] in the (a)–(c) viscous sublayer and the (d)–(f) log region. Black lines are the same as Fig. 12.

In Fig. 14 we report the results of supersonic/hypersonic turbulent boundary layers [18,38] for the [Figs. 14(a)–14(c)] viscous sublayer and the [Figs. 14(d)–14(f)] log region separately. To facilitate comparison, in Figs. 14(a)–14(c), the cases with y_c^* within the viscous sublayer are eliminated, and the profiles of the compressible cases in Figs. 14(d)–14(f) are shifted to match the incompressible one at $y^+ = 50$ or $y^* = 50$. It can be seen that θ_{SL}^+ ($\theta_{SL,m}^+$) and θ_S^+ ($\theta_{S,m}^+$) are closer to the incompressible profile in the viscous sublayer than θ_{VD}^+ ($\theta_{VD,m}^+$). In the log region, the performance of θ_S^+ ($\theta_{S,m}^+$) is the most outstanding. As a side note, there is some scatter from the reference data in Figs. 14(b) and 14(c) in the upper boundary of the viscous sublayer for $\theta_{S,L}^+$ ($\theta_{SL,m}^+$) and θ_S^+ ($\theta_{S,m}^+$). This is expected because the temperature distribution in a boundary layer with cold wall is nonmonotonic.

For modeling purposes, Patel *et al.* [15] pointed out that a mean temperature profile can be further transformed into another one based on ϕ_{TL},

$$\theta_{\tau,SL}^+ = \int \phi_{\tau,SL} \, dy^*, \tag{33}$$

where

$$\phi_{\tau,SL} = \phi_{SL} \frac{1/\mathrm{Pr} + \alpha_t/\bar{\mu}}{1 + \alpha_t/\bar{\mu}}. \tag{34}$$

According to Eq. (13), in the vicinity of the wall, $\theta_\tau^+ = y^*$, whereas in the log region, $\theta_\tau^+ = \kappa_t^{-1}\ln(y^*) + C$ (C is a constant, and roughly equivalent to 6.5). This transformation is based on the Mach number invariant of ψ_3, and can diminish the Prandtl-number dependence of the transformed profile.

Here we propose another transformation of this type based on our proposed function ϕ_S:

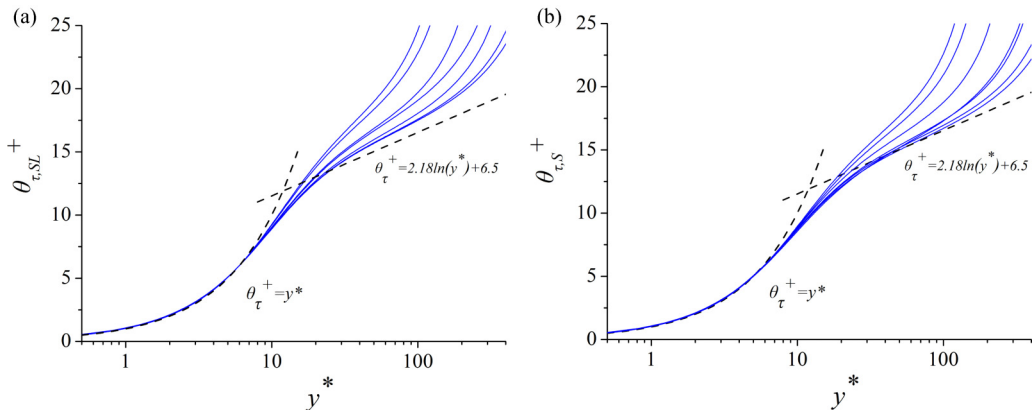$$\theta_{\tau,S}^+ = \int \phi_{\tau,S} \, dy^*, \tag{35}$$

FIG. 15. Temperature profiles transformed (a) $\theta_{\tau,SL}^+$ and (b) $\theta_{\tau,S}^+$ for compressible channel flows with adiabatic walls [37].

where

$$\phi_{\tau,S} = \phi_{S,m}\frac{1/\mathrm{Pr} + \alpha_t/\bar{\mu}}{1 + \alpha_t/\bar{\mu}}. \tag{36}$$

According to the discussions above, it can be conjectured that $\theta_{\tau,S}^+$ would be closer to the prediction than $\theta_{\tau,SL}^+$ for compressible channel flows with adiabatic walls. The assertion is validated in Fig. 15, where $\theta_{\tau,SL}^+$ and $\theta_{\tau,S}^+$ of compressible channel flows with adiabatic walls are compared. It can be seen that $\theta_{\tau,S}^+$ are closer to the prediction as the increase of the Reynolds number.

VI. CONCLUDING REMARKS AND OUTLOOK

In the present study, we compare the semilocal-type (ϕ_{SL}), van Driest-type (ϕ_{VD}) scalings, and the invariant function proposed by the present study (ϕ_S) associated with the mean temperature field in compressible wall turbulence case by case. ϕ_{SL} works well in the inner layer of compressible channel flows with isothermal walls; ϕ_S works well in the inner layer of compressible channel flows with adiabatic walls, and supersonic/hypersonic turbulent boundary layers with cold walls; ϕ_{VD} does not work the best among all three functions in the flows under consideration. The high-order terms are shown to influence the scaling in the viscous sublayer of supersonic/hypersonic turbulent boundary layers with cold walls and channel flows over adiabatic walls. Upon this understanding, we propose temperature transformations based on ϕ_S, which show an improvement in channel flows over adiabatic walls and supersonic/hypersonic turbulent boundary layers with cold walls.

It can be observed that the temperature field is more challenging to model than the velocity field. The current study gives some insights into the mean temperature scaling. However, we want to acknowledge that the current work, as well as the previous ones by other groups, is not perfect. There are some issues remaining to be settled:

(a) Is there a unified Mach invariant function for all kinds of flows under consideration?

(b) Is there a more general transformation for the flows with nonmonotonic temperature distributions? Especially, how can we model the nonmonotonicity of a temperature profile?

We hope the present study, along with these open questions, can be instructive for near-wall modeling in high-speed aerodynamics and trigger new studies on this significant topic.

APPENDIX: DIMENSION ANALYSIS OF EQ. (2)

According to Cebeci [28], the dimensions of the physical quantities appeared in Eq. (2) are

$$\rho = O(1), \quad u = O(1), \quad v = O(1), \quad H = O(1), \quad T = O(1), \quad h = O(1), \quad \partial/\partial x = O(1),$$

$$\partial/\partial y = O(h^{-1}), \quad \lambda = O(h^2), \quad \mu = O(h^2), \ \rho H'' = O(h), \quad \rho H'' u'' = O(h), \quad \rho H'' v'' = O(h),$$
$$\tag{A1}$$

where h denotes the boundary layer thickness, and $h \ll 1$. Apparently, the left-hand side of Eq. (2) is $O(1)$. The dimensions of the two terms on the right-hand side can also be estimated by evaluating each component individually. Only the leading-order component with $O(1)$ is dominant:

$$\frac{\partial \bar{q}_x}{\partial x} = O(h^2), \quad \frac{\partial \overline{\rho H'' u''}}{\partial x} = O(h), \quad \frac{\partial \overline{u \tau_{xx}}}{\partial x} = O(h^2), \quad \frac{\partial \overline{v \tau_{yx}}}{\partial x} = O(h^2),$$

$$\frac{\partial \bar{q}_y}{\partial y} = O(1), \quad \frac{\partial \overline{\rho H'' v''}}{\partial y} = O(1), \quad \frac{\partial \overline{u \tau_{xy}}}{\partial y} = O(1), \quad \frac{\partial \overline{v \tau_{yy}}}{\partial y} = O(h^2). \tag{A2}$$

Hence, Eq. (2) can be simplified by neglecting the high-order terms, which yields

$$\frac{\partial (\bar{\rho} \tilde{H} \tilde{u})}{\partial x} + \frac{\partial (\bar{\rho} \tilde{H} \tilde{v})}{\partial y} = \frac{\partial}{\partial y} (\bar{q}_y - \overline{\rho H'' v''} + \overline{u \tau_{xy}}). \tag{A3}$$

Equation (A3) can be further simplified by taking no account of the streamwise development of the boundary layer, and assuming the one-dimensionality of the flow,

$$\frac{\partial}{\partial y} (\bar{q}_y - \overline{\rho H'' v''} + \overline{u \tau_{xy}}) = 0. \tag{A4}$$

---

[1] B. Kader, Temperature and concentration profiles in fully turbulent boundary layers, Int. J. Heat Mass Transf. **24**, 1541 (1981).

[2] S. Pirozzoli, An explicit representation for mean profiles and fluxes in forced passive scalar convection, J. Fluid Mech. **968**, R1 (2023).

[3] L. Fu, M. Karp, S. Bose, P. Moin, and J. Urzay, Shock-induced heating and transition to turbulence in a hypersonic boundary layer, J. Fluid Mech. **909**, A8 (2021).

[4] L. Fu, S. Bose, and P. Moin, Prediction of aerothermal characteristics of a generic hypersonic inlet flow, Theor. Comput. Fluid Dyn. **36**, 345 (2022).

[5] T. Bai, C. Cheng, and L. Fu, Effects of mean shear on the vortex identification and the orientation statistics, Theor. Appl. Mech. Lett. **13**, 100454 (2023).

[6] M. Morkovin, Effects of compressibility on turbulent flows, *Mécanique de la Turbulence*, edited by A. Favre (CNRS, 1969).

[7] E. R. Van Driest, Turbulent boundary layer in compressible fluids, J. Aeronaut. Sci. **18**, 145 (1951).

[8] Y.-S. Zhang, W.-T. Bi, F. Hussain, X.-L. Li, and Z.-S. She, Mach-number-invariant mean-velocity profile of compressible turbulent boundary layers, Phys. Rev. Lett. **109**, 054502 (2012).

[9] A. Trettel and J. Larsson, Mean velocity scaling for compressible wall turbulence with heat transfer, Phys. Fluids **28**, 026102 (2016).

[10] A. Patel, B. Boersma, and R. Pecnik, The influence of near-wall density and viscosity gradients on turbulence in channel flows, J. Fluid Mech. **809**, 793 (2016).

[11] P. S. Volpiani, P. S. Iyer, S. Pirozzoli, and J. Larsson, Data-driven compressibility transformation for turbulent wall layers, Phys. Rev. Fluids **5**, 052602 (2020).

[12] K. Griffin, L. Fu, and P. Moin, Velocity transformation for compressible wall-bounded turbulent flows with and without heat transfer, Proc. Natl. Acad. Sci. USA **118**, e2111144118 (2021).

[13] T. Bai, K. Griffin, and L. Fu, Compressible velocity transformations for various noncanonical wall-bounded turbulent flows, AIAA J. **60**, 4325 (2022).

[14] K. Younes and J. J. Hickey, Mean velocity scaling of high-speed turbulent flows under nonadiabatic wall conditions, AIAA J. **61**, 1532 (2023).

[15] A. Patel, B. J. Boersma, and R. Pecnik, Scalar statistics in variable property turbulent channel flows, Phys. Rev. Fluids **2**, 084604 (2017).

[16] P. E. S. Chen, Y. Lv, H. A. Xu, Y. Shi, and X. I. A. Yang, LES wall modeling for heat transfer at high speeds, Phys. Rev. Fluids **7**, 014608 (2022).

[17] P. Chen, G. Huang, Y. Shi, X. Yang, and Y. Lv, A unified temperature transformation for high-Mach-number flows above adiabatic and isothermal walls, J. Fluid Mech. **951**, A38 (2022).

[18] C. Zhang, L. Duan, and M. Choudhari, Direct numerical simulation database for supersonic and hypersonic turbulent boundary layers, AIAA J. **56**, 4297 (2018).

[19] C. Cheng, X. Chen, W. Zhu, W. Shyy, and L. Fu, Progress in physical modeling of compressible wall-bounded turbulent flows, Acta Mech. Sin. **40**, 323663 (2024).

[20] A. Busemann, *Handbuch der Experimentalphysik* (Geest und Portig, Leipzig, 1931), Vol. 4.

[21] L. Crocco, Sulla trasmissione del calore da una lamina piana a un fluido scorrente ad alta velocita, L'Aerotecnica **12**, 181 (1932).

[22] A. Walz, *Boundary Layers of Flow and Temperature* (MIT Press, Cambridge, MA, 1969).

[23] L. Duan and M. Martin, Direct numerical simulation of hypersonic turbulent boundary layers. Part 4. Effect of high enthalpy, J. Fluid Mech. **684**, 25 (2011).

[24] Y. Zhang, W. Bi, F. Hussain, and Z. She, A generalized Reynolds analogy for compressible wall-bounded turbulent flows, J. Fluid Mech. **739**, 392 (2014).

[25] Y. Song, P. Zhang, Y. Liu, and Z. Xia, Central mean temperature scaling in compressible turbulent channel flows with symmetric isothermal boundaries, Phys. Rev. Fluids **7**, 044606 (2022).

[26] K. Griffin, L. Fu, and P. Moin, Near-wall model for compressible turbulent boundary layers based on an inverse velocity transformation, J. Fluid Mech. **970**, A36 (2023).

[27] S. Kawai and J. Larsson, Wall-modeling in large eddy simulation: Length scales, grid resolution, and accuracy, Phys. Fluids **24**, 015105 (2012).

[28] T. Cebeci, *Analysis of Turbulent Boundary Layers* (Elsevier, New York, 1974).

[29] K. Younes, Velocity scaling of high-speed turbulent boundary layer flows with wall heat transfer, Master's thesis, University of Waterloo, 2021.

[30] A. Smits and J. Dussauge, *Turbulent Shear Layers in Supersonic Flow* (Springer Science & Business Media, 2006).

[31] P. Huang, G. Coleman, and P. Bradshaw, Compressible turbulent channel flows: DNS results and modelling, J. Fluid Mech. **305**, 185 (1995).

[32] W. Li, Y. Fan, D. Modesti, and C. Cheng, Decomposition of the mean skin-friction drag in compressible turbulent channel flows, J. Fluid Mech. **875**, 101 (2019).

[33] C. Cheng and L. Fu, Linear-model-based study of the coupling between velocity and temperature fields in compressible turbulent channel flows, J. Fluid Mech. **964**, A15 (2023).

[34] X. Chen, C. Cheng, L. Fu, and J. Gan, Linear response analysis of supersonic turbulent channel flows with a large parameter space, J. Fluid Mech. **962**, A7 (2023).

[35] C. Cheng, W. Shyy, and L. Fu, Momentum and heat flux events in compressible turbulent channel flows, Phys. Rev. Fluids **8**, 094602 (2023).

[36] F. Alcántara-Ávila, S. Hoyas, and M. J. Pérez-Quiles, Direct numerical simulation of thermal channel flow for $Re_\tau = 5000$ and $Pr = 0.71$, J. Fluid Mech. **916**, A29 (2021).

[37] D. J. Lusher and G. N. Coleman, Numerical study of compressible wall-bounded turbulence—The effect of thermal wall conditions on the turbulent Prandtl number in the low-supersonic regime, Int. J. Comput. Fluid Dyn. **36**, 797 (2023).

[38] M. Cogo, F. Salvadore, F. Picano, and M. Bernardini, Direct numerical simulation of supersonic and hypersonic turbulent boundary layers at moderate-high Reynolds numbers and isothermal wall condition, J. Fluid Mech. **945**, A30 (2022).

[39] P. Huang, G. Coleman, P. Spalart, and X. Yang, Velocity and temperature scalings leading to compressible laws of the wall, J. Fluid Mech. **977**, A49 (2023).